JOURNAL OF Applied Polymer SCIENCE

Synthesis and characterization of crosslinked polyurethane/clay nanocomposites

Shirley Peng, Jude O. Iroh
Department of Mechanical and Materials Engineering, University of Cincinnati, Cincinnati, Ohio 45221
Correspondence to: J. O. Iroh (E-mail: irohj@ucmail.uc.edu)

ABSTRACT: A series of glycerin-crosslinked polyurethane (XPU)-clay nanocomposites were prepared by *in situ* polymerization followed by solution casting and thermal treatment. The weight percent (wt %) of clay in the nanocomposites was varied between 0.25 and 10. The structural, rheological and dynamic mechanical properties of the nanocomposites were investigated. X-ray diffraction (XRD) analysis showed that well dispersed clay platelets were formed in nanocomposites containing up to 1 wt % of clay. Scanning electron microscopy (SEM) showed that poorly dispersed and non-exfoliated clays were present in composites containing >2 wt % of clay and resulted in phase-separated disparities within the matrix. Rheological studies demonstrated that processability of polyurethane was significantly improved after clay addition such that solution viscosity decreased by between 76 and 90%. Furthermore, the presence of chemical and physical crosslink networks within the matrix resulted in a remarkable enhancement in the rubbery plateau storage modulus. © 2016 Wiley Periodicals, Inc. J. Appl. Polym. Sci. **2016**, *133*, 43346.

KEYWORDS: clay; composites; polyurethanes; synthesis and processing

Received 30 June 2015; accepted 12 December 2015
DOI: 10.1002/app.43346

INTRODUCTION

Polymer-clay nanocomposites have received a lot of attention because of their ability to improve the mechanical, thermal and barrier properties of conventional polymers.[1–4] Montmorillonite (MMT) clay has been extensively used to reinforce polymers due to its high aspect ratio, rich intercalation chemistry and relatively low cost.[5]

In its natural state, the unit cell of MMT is comprised of octahedral alumina sheet sandwiched between two silica tetrahedral sheets. The trivalent aluminum ions, Al^{3+} is partially substituted by divalent ferrous, Fe^{2+} or magnesium, Mg^{2+} resulting in shortage of positive charge and partial negative charge for the crystal lattice. Organic cationic surfactants are often added to increase the hydrophobicity of surface, there-by making it compatible with organic polymer materials.[6,7] The dispersion of clay in a polymer matrix can result in any of the three structural forms including agglomerated (conventional), intercalated, and exfoliated.[6–8]

When layered clay platelets are incompatible with the polymer matrix, the platelets will tend to aggregate and result in conventional form. When the polarities of two materials are similar, clay sheets can become intercalated or exfoliated. Intercalation involves the insertion of polymer chains within the gallery of the clay contributing to expansion of the interlayer spacing. Full separation and delamination of platelets result in exfoliation.[6,8]

After the pioneering work in nylon-clay nanocomposites at Toyota,[9] a plethora of studies focused on polymer–clay nanocomposites followed.[10–18] Nanocomposites based on polyurethane and MMT clay is one area that has been highly investigated.[10] Polyurethanes (PU) are versatile materials possessing advantageous properties such as high abrasion strength, elasticity, and flexibility. Polyurethane's properties are highly influenced by their unique phase-separated morphology consisting of a long, flexible unit and a short, hard unit. However, their structure contributes to their poor barrier properties.[11–14] To compensate for this drawback, MMT clay is incorporated into the PU matrix.[15] Additionally, chemical crosslinks can be introduced into the matrix during curing to form a 3D network structure.[16]

In the past, researchers have studied few features of crosslinked PU-clay nanocomposite systems. For example, Ma *et al.*,[17] showed that clay improved tensile properties of glycerol propoxylate (GP) crosslinked PU. While others such as Rama *et al.*,[18] investigated the effect of trimethylol propane (TMP) crosslinked PU on the dispersability of clay.

In this article, we report the synthesis, rheology, and dynamic mechanical behavior of crosslinked PU–clay nanocomposites. It was demonstrated that MMT clay improved the processability of PU by significantly reducing PU solution viscosity. Additionally, MMT clay was shown to enhance both the glassy region and rubbery plateau region storage modulus of PU. A correlation between

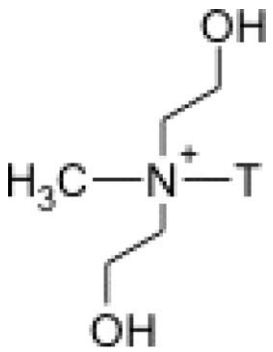

Figure 1. Chemical structure of the organic modifier for C30B. Where *T* is Tallow (~65% C_{18}, ~30% C_{16}, ~5% C_{14}) and the anion is chloride ion.

the morphology and dynamic mechanical behavior of the nanocomposites was made.

EXPERIMENTAL

Materials

Polytetrahydrofuran (PTHF) (M_n ~1000 g mol^{-1}), 4, 4′-methylenebis(phenyl isocyanate) (MDI) and anhydrous *N*,*N*-dimethylformamide (DMF) were purchased from Sigma–Aldrich. Certified A.C.S. grade glycerin (propane-1,2,3-triol) was obtained from Fisher Scientific. Cloisite 30B^{TM} (C30B), a MMT clay commercially treated with a methyl, dehydrogenated tallow (Composed of ~65% C18, ~30% C16 and ~5% C14)[19] ammonium shown in Figure 1, was supplied by Southern Clay Products and dried in the oven at 100°C for 24 h prior to use.

Preparation of Neat XPU

In a three-neck flask, 10 mmol of PTHF was dissolved in 100 mL DMF and heated to 60°C in a water bath under a steady flow of nitrogen. To the solution, 20 mmol of MDI was added under stirring and allowed to react for 1 h to form a NCO-terminated prepolymer. The mixture was maintained at 60°C and 6 mmol of glycerin was added dropwise and stirred for 10 min. Afterward, the solution was stirred for an additional 30 min at room temperature to form branched PU. The whole solution was poured into a Teflon mold and solvent removed at 70°C for 24 h to fully cure and crosslink the material.

Preparation of XPU–Clay Nanocomposites

XPU–clay nanocomposites were prepared by *in situ* polymerization. PTHF was first dissolved in a three-neck flask containing 100 mL DMF at room temperature. Different quantities of clay by weight (Table I) were added to the solution under rapid stirring for 2h followed by sonication for 1 h to completely disperse the clay. The mixture was then heated to 60°C under nitrogen atmosphere and polymerization was carried out in the same manner as described in the preparation of neat XPU subsection above. The schematic showing the preparation of XPU–clay suspension is shown in Figure 2.

Characterization

Fourier-Transform Infrared (FTIR) Spectroscopy was used to probe the structure of cured samples. A total of 32 scans were collected on a Thermo Scientific Nicolet 6700 spectrometer in the 4000–400 cm^{-1} wavenumber range. OMNIC 32 software was used to analyze the spectra.

Table I. Designated Sample Names with Their Corresponding Filler Content

Sample name	Clay concentration (wt %)
Neat XPU	0
XPU-C025	0.25
XPU-C05	0.5
XPU-C1	1
XPU-C2	2
XPU-C5	5
XPU-C10	10

The dispersion of clay was studied using a PANalytical X'Pert Pro diffractometer operating at 45 kV and 40 mA. Scans were performed in the range between 2° and 7° with a Cu Kα radiation source of wavelength equal to 1.54 Å. The *d*-spacing of clay was calculated using Braggs Law.[20]

$$d = \frac{n\lambda}{2\sin\theta}$$

Where n is a constant equal to 1, λ is the wavelength of radiation, and θ is the angle of diffraction.

Rheological measurement was done in a rotational Brookfield DV-I+ Viscometer. A container diameter of 18.66 mm and S31 spindle with diameter of 5.88 mm was used. Viscosity measurements were carried out at spindle speeds between 5 and 100 rpm. To correlate viscosity with the shear rate, the following equation was used.[21]

$$S\ (s^{-1}) = \frac{2\omega Rc^2}{(Rc^2 - Rb^2)}$$

where ω is the conversion factor, R_c is the container radius and R_b is the spindle radius. The conversion factor can be described by using the formula below.[21]

$$\omega\ (rad/s) = \frac{2\pi(\text{speed})}{60}$$

Dynamic mechanical spectrometry (DMS, Seiko Instruments SII EXSTAR 6000) was utilized to provide evidence for the crosslinking of PU and analyze thermo-mechanical properties. Free-standing rectangular films were tested between −100°C and 50°C at a heating rate of 5°C min^{-1} and frequency of 1 Hz.

RESULTS

Structural Characterization

Figure 3 shows the FTIR spectra of the monomers and neat XPU. The isocyanate group (—NCO) is observed at 2281 cm^{-1} in the MDI spectrum and reactive hydroxyl groups (—OH) in the PTHF and glycerin spectra are shown at 3457 and 3346 cm^{-1}. In the neat XPU, the disappearance of isocyanate and hydroxyl groups demonstrated that all monomers reacted during polymerization. In turn, the appearance of new peaks at 1223, 1730, and 3309 cm^{-1} is attributed to C—O, C═O, and N—H stretch, respectively confirming the formation of urethane groups. Further assignment of polyurethane peaks are provided in Table II.[22]

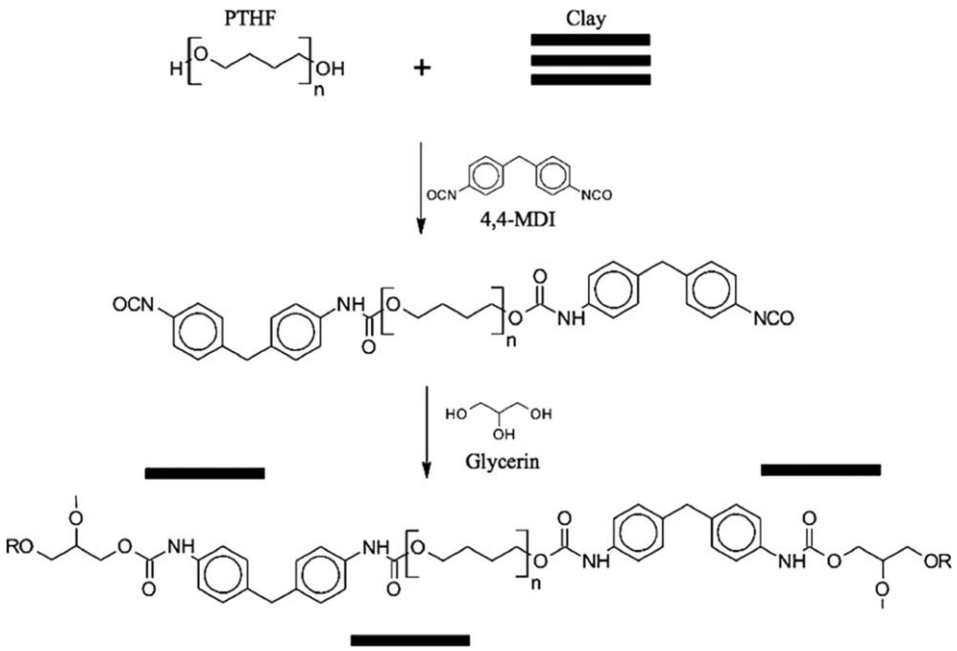

Figure 2. Formation of XPU–clay nanocomposites.

Figure 4 shows the spectrum of C30B clay. At low wavenumbers of 461 and 522 cm^{-1}, peaks arise due to inorganic moieties within the clay. Peaks observed at 919, 1043, and 3626 $cm^{-1}$are due to Al—OH—Al deformation, Si—O—Si stretch and silicate O—H stretch, respectively. The peaks at 1469, 2851, and 2923 $cm^{-1}$are due to CH_2 stretched from the organic modifier.

In Figure 5, incorporation of clay into neat XPU led to the appearance of clay absorption peak for samples with clay concentrations above 2 wt %. With the addition of clay, characteristic polyurethane peaks are still observed around the 1223, 1730, and 3300 cm^{-1} regions confirming that clay did not obstruct the formation of polyurethane.

Because Cloisite 30B clay has the ability to physically interact with urethane groups, the extent of hydrogen bonding within the system as clay content increased was studied. To do so, ratio of the area under the 1709 and 1730 cm^{-1} peaks associated with hydrogen bonded carbonyl and free carbonyl groups, respectively, were calculated using the equation below.

Table II. Assigned Characteristic Peaks for Neat XPU

Wavenumber (cm^{-1})	Characteristic peak
1111	ν_s(CO)
1223	ν_s(CO)
1310	ν_s(C—N)
1538	ν_b(NH) and ν_s(O=C=N)
1597	ν_s(C=C)
1708	ν_s(C=O)
1730	
2796	ν_s(CH) and ν_s(CH_2)
2858	
2941	
3309	ν_s(NH)

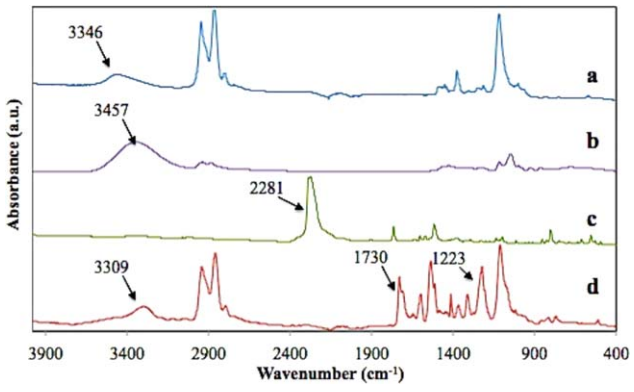

Figure 3. FTIR spectra of (a) PTHF, (b) glycerin, (c) MDI, and (d) neat XPU. [Color figure can be viewed in the online issue, which is available at wileyonlinelibrary.com.]

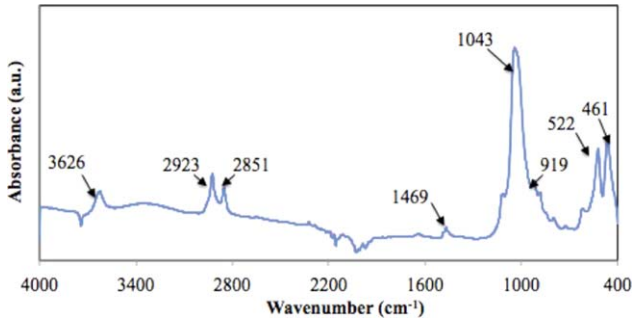

Figure 4. FTIR spectrum of Cloisite C30B clay. [Color figure can be viewed in the online issue, which is available at wileyonlinelibrary.com.]

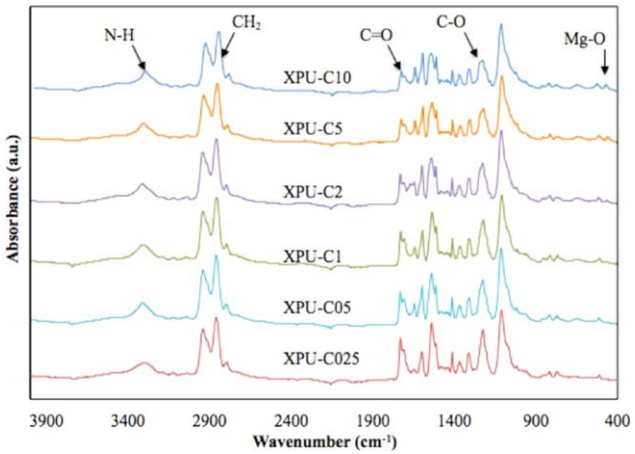

Figure 5. FTIR spectra of XPU–clay nanocomposites. [Color figure can be viewed in the online issue, which is available at wileyonlinelibrary.com.]

$$Ratio = \frac{A_{1709}/A_{1597}}{A_{1730}/A_{1597}}$$

The area of the 1597 cm^{-1} peak due to C═C stretching of the benzene ring was used to normalize the area of the carbonyl absorption peaks.

As shown in Figure 6, hydrogen bonding was greatest at clay loading between 0.25 and 1 wt %. At 2 wt % clay, the hydrogen bonding intensity sharply decreased. XPU-clay intercalation could be a source for this behavior such that at concentrations higher than 1 wt %, clay layers become poorly dispersed leading to a decrease in surface area and weaker interactions with urethane linkages. At 10 wt % clay, the hydrogen interactions slightly increased most likely due to higher concentration of clay within the system and less to do with clay dispersion.

Clay Dispersion

Figures 7(a–c) show the diffraction patterns of C30B clay, neat XPU and XPU-clay nanocomposites. The C30B clay shows a strong diffraction peak at 2θ of 4.78° with *d*-spacing of 18.5 Å, which coincides with values reported by others.[23] At low clay concentrations up to 1 wt %, no peaks were observed in the diffractograms indicating that clay is uniformly dispersed in XPU and that there are no agglomerates of clay in the matrix at a low concentration of clay.

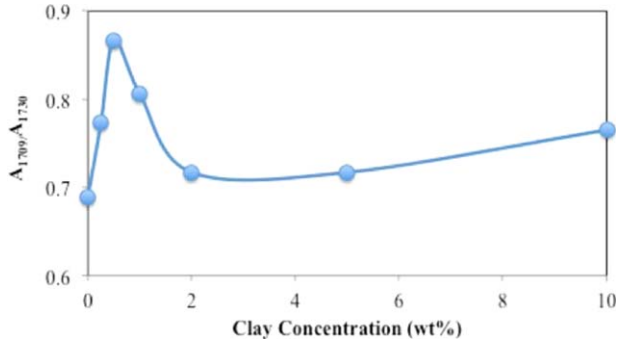

Figure 6. Hydrogen bonding index based on the ratio of carbonyl peaks absorption area at different clay loading. [Color figure can be viewed in the online issue, which is available at wileyonlinelibrary.com.]

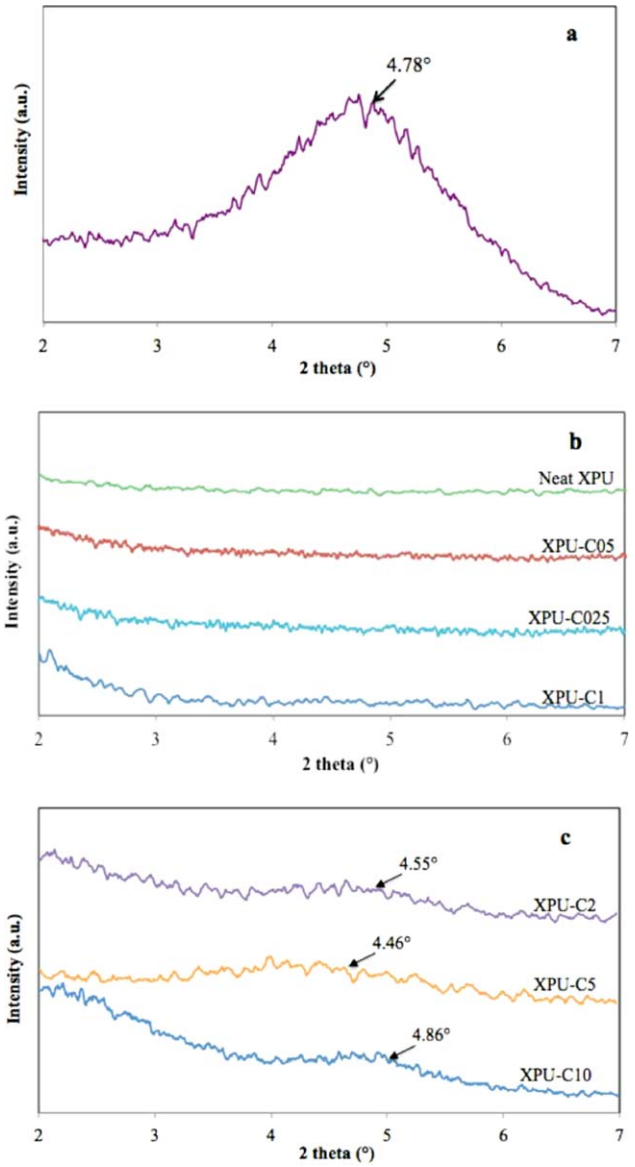

Figure 7. XRD of (a) C30B (b) neat XPU and nanocomposites at clay concentrations between 0.25 and 1 wt % and c) nanocomposites with clay concentrations between 2 and 10 wt %. [Color figure can be viewed in the online issue, which is available at wileyonlinelibrary.com.]

The diffractograms for composites containing 2, 5, and 10 wt % of clay shows a weak and broad peak at 2θ of 4.55° with *d*-spacing of 19.4 Å, 2θ of 4.46° with *d*-spacing of 19.8 Å and 2θ of 4.86 with *d*-spacing of 18.1 Å, respectively. For nanocomposites containing 2 and 5 wt % clay, the gallery spacing increased in comparison to C30B clay indicating that intercalation occurred and that XPU chains were inserted between the clay layers. However, at 10 wt % clay, the *d*-spacing slightly decreased below the *d*-spacing of neat powder clay indicating the clay may exist in both intercalated and conventional form. It is assumed that clay aggregation would cause clay platelets to move closer together resulting in smaller gallery spacing and slight upward shift in the diffraction angle (2θ).[24,25]

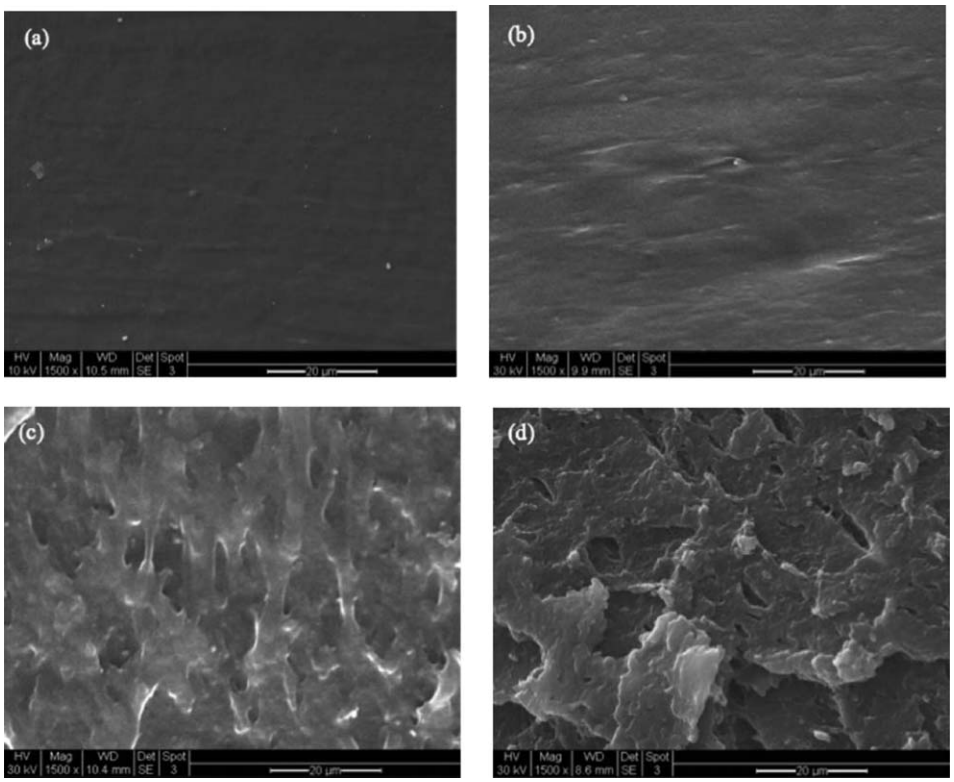

Figure 8. Cross-sectional SEM images of (a) neat XPU, (b) XPU-C1, (c) XPU-C2, and (d) XPU-C10 at ×1500.

Scanning Electron Microscopy

The cross-sectional morphology of neat XPU, XPU-C1, XPU-C2, and XPU-C10 can be observed in Figure 8(a–d). In the neat XPU and 1 wt % clay nanocomposite, a homogenous matrix was observed. As clay loading reached 2 wt %, slight fibrous-like structures were present, indicating the occurrence of phase-separation. Phase-separation behavior was likely caused by intercalated clay existing within the nanocomposite. This would correlate well with results reported from XRD analysis. Clay exhibiting intercalated structures are only moderately dispersed as they still maintain some crystallinity and stacks of silicate layers within their structure. By increasing the clay concentration to 10 wt %, greater amounts of voids were observed indicating that clay may play a role in facilitating phase-separation. Furthermore, the appearance of a rough morphology can serve as an indication that the bulk morphology of the matrix was dominated by clay.

Rheology

The rheological behavior of neat XPU and XPU–clay nanocomposite solutions at varied temperatures are shown in Figure 9(a,b). At 25°C Newtonian behavior was observed for all samples. When the temperature was increased to 70°C, shear-thinning behavior occurred. In addition, fluctuations in viscosity as shear rate increased were observed in nanocomposite solutions. This behavior could be due to the direct effect of clay-urethane interactions where strong interactions would cause slight increases in viscosity upon a change in shear rate. Furthermore, the addition of clay led to a noticeable decrease in overall viscosity in comparison to neat XPU at 25 and 70°C. This reduced viscosity can be explained by clay platelets limiting interactions between monomers during polymerization,[24] which would lead to lower molecular weight chains being formed. This suggests that processability of XPU solution was greatly improved as higher concentrations of clay are added.

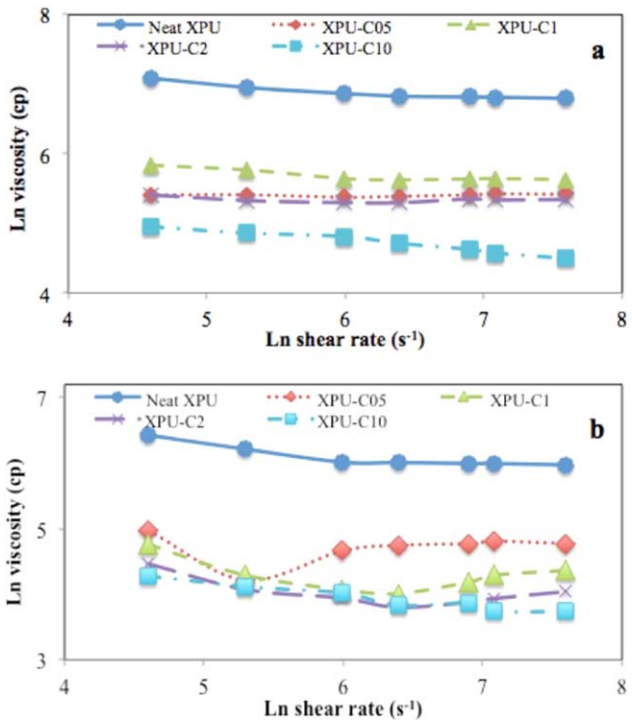

Figure 9. Simple shear viscosity of neat XPU solution and nanocomposite suspensions at (a) 25°C and (b) 70°C. [Color figure can be viewed in the online issue, which is available at wileyonlinelibrary.com.]

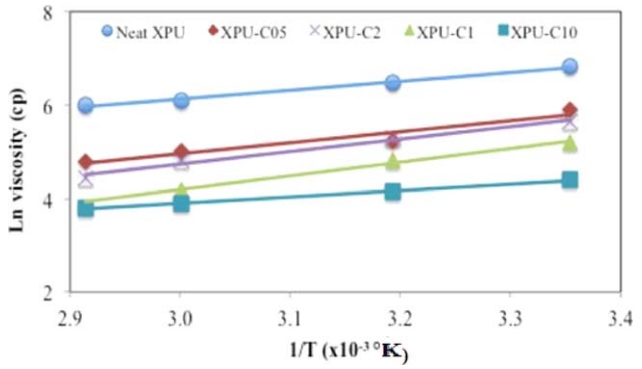

Figure 10. Viscosity of the neat XPU solution and nanocomposite suspensions as a function of temperature and composition. [Color figure can be viewed in the online issue, which is available at wileyonlinelibrary.com.]

The energy required for viscous flow of polymer solutions was determined by using the Arrhenius equation shown below, which describes how viscosity varies with temperature at constant shear rate.[26]

$$\eta = Ae^{\frac{E_a}{RT}}$$

The variables, η, A, E_a, R, and T represent viscosity of solution, Arrhenius constant, activation energy, gas constant, and absolute temperature, respectively. Linearization of this equation can be achieved by taking the natural log of both sides, as represented below.[26]

$$\ln \eta = \frac{E_a}{RT} + \ln A$$

By plotting ln η vs. $1/T$ (Figure 10), the activation energy can be attained by multiplying the slope with gas constant.

Table III shows the calculated activation energy for the respective samples. It is shown that as clay content increased to 2 wt %, the energy required for viscous flow was greatest. Thereafter, increasing the clay to 10 wt % resulted in a decrease in the activation energy. Because activation energy is dependent on how temperature influences viscosity changes, it can be assumed that at 1 wt % clay loading, the system exhibited the greatest thermal sensitivity due to more urethane–clay bonds being broken as temperature increases.

Dynamic Mechanical Spectroscopy

Figure 11(a,b) represent the changes in storage modulus and tan δ with temperature for linear PU, neat XPU and selected PU nanocomposites. The linear PU composed of PTHF, MDI, and 1,4-butanediol was utilized to differentiate linear PU from neat crosslinked XPU system.

As observed in the storage modulus versus temperature plot, the neat XPU exhibited a higher glassy region storage modulus and rubbery plateau modulus than the linear PU, indicating higher stiffness and crosslink density in the neat XPU system. By adding clay into the crosslinked system, an increase in overall storage modulus was observed, indicating an increase in rigidity of XPU. These enhancements in the storage modulus were attributed to chemical and physical interactions existing between the clay and urethane groups. At high clay concentrations of 10 wt % clay, it is believed that the large increase in rubbery plateau modulus may be due to the rigid filler causing elastic disparities within the matrix.[27]

Table III. Activation Energies of XPU–Clay Nanocomposites

Sample	E_a (kJ mol^{-1})
Neat XPU	15.8
XPU-C025	16.8
XPU-C05	18.0
XPU-C1	26.5
XPU-C2	22.2
XPU-C5	10.9
XPU-C10	8.9

The glass-transition region, which represents the temperature range at which long-range molecular motion occurs in the polymer backbone, demonstrated that up to 1 wt % clay concentration, a narrow and sharp decrease in modulus was observed. By increasing clay concentration to 10 wt %, a broad glass transition was observed. This broadness was correlated to phase-separation present within the nanocomposite, as previously observed in SEM analysis. Because the nanocomposite possessed clay aggregates within the matrix, it is assumed that the first decrease in the glass-transition region was due to chain motion

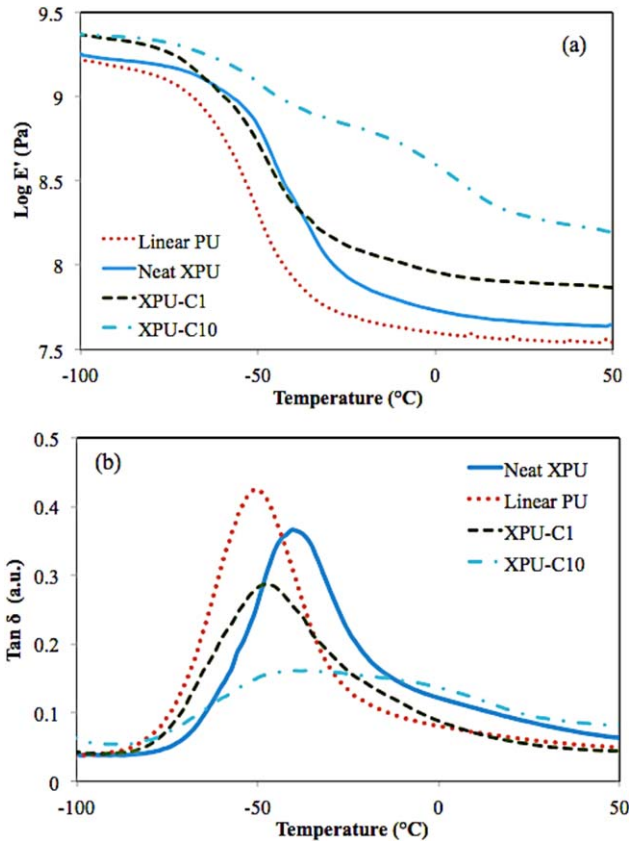

Figure 11. Dependence of (a) storage modulus and (b) tan delta on temperature and composition for linear PU, neat XPU, PU-C1, and XPU-C10. [Color figure can be viewed in the online issue, which is available at wileyonlinelibrary.com.]

in XPU matrix and the succeeding decrease was due to clay-urethane interfacial interactions.

The tan δ vs. temperature plot (Figure 11b), for the neat XPU showed a lower tan delta height for the α-transition than the linear PU indicating lower damping ability due to imposed constraint to chain mobility of the polyurethane. This effect is characteristic presence of crosslinks in a polymer. As clay was added introduced to the XPU, a broadened α-transition peak was observed. This is believed to be due to reduced homogeneity in the nanocomposite. The tan δ peaks for α-transition also showed that the neat XPU and linear PU had glass-transition temperature (T_g) at -43°C and -53°C, respectively. This observed property correlated with data reported by Chiou *et al.*,[28] in which increased crosslink density directly resulted in increased T_g. In relation to the neat XPU, the XPU-C10 showed two T_g's at -48°C and -3.7°C. The decrease in initial T_g was likely an effect of clay decreasing the formation of chemical crosslink networks during curing as its platelets reduced contact between reactive groups.

CONCLUSIONS

Crosslinked polyurethane nanocomposites containing varied concentrations of clay were successfully synthesized via *in situ* polymerization. Upon clay addition, processability was enhanced as a significant reduction in viscosity was achieved. In XRD and SEM analysis, it was observed that low concentrations of clay resulted in a higher degree of dispersion, whereas the aggregation of clay facilitated phase-separation behavior. Correlation of these findings with dynamic mechanical behavior showed that homogenous distribution of clay in the nanocomposites resulted in a narrow glass-transition region while phase-separated materials produced broadened glass transition regions. Additionally, incorporation of clay enhanced both the glassy region storage modulus and the rubbery plateau storage modulus due to enhanced chemical and physical interactions. The use of a combination of dynamic mechanical spectroscopy and X-ray diffraction method to study the composites enabled a correlation between the microstructure of clay filled crosslinked polyurethane and their dynamic mechanical behavior to be uncovered.

ACKNOWLEDGMENTS

The authors thank Dr. Necati Kaval, Dr. Pablo Rosales, and Fei Yu for their instrumentation assistance.

REFERENCES

1. Paul, D. R.; Robeson, L. M. *Polymer* **2008**, *49*, 3187.
2. Jordan, J.; Jacob, K. I.; Tannenbaum, R.; Sharaf, M. A.; Jasiuk, I. *Mater. Sci. Eng. A* **2005**, *393*, 1.
3. Okada, A.; Usuki, A. *Macromol. Mater. Eng.* **2006**, *291*, 1449.
4. Gilman, J. W. *Appl. Clay Sci.* **1999**, *15*, 31.
5. Grigoriadi, K.; Giannakas, A.; Ladavos, A.; Barkoula, N. M. *Polym. Eng. Sci.* **2012**, *53*, 301.
6. Kedzierski, M.; Penczek, P. *Polimery* **2004**, *49*, 801.
7. Ray, S. S.; Okamoto, M. *Prog. Polym. Sci.* **2003**, *28*, 1539.
8. Factor, M. J.; Lee, S. In Particle Technology and Applications; Lee, S., Henthorn, K. H., Eds.; CRC Press: Florida, **2012**; Vol. *1*, Chapter 15, p 235.
9. Kojima, Y.; Usuki, A.; Kawasumi, M.; Okada, A.; Kurauchi, T.; Kamigaito, O. *J. Polym. Sci. A Polym. Chem.* **1993**, *31*, 1755.
10. Saha, C.; Chaki, T. K.; Singha, N. K. *J. Appl. Polym. Sci.* **2013**, *130*, 3328.
11. Ha Thuc, C. N.; Cao, H. T.; Nguyen, D. M.; Tran, M. A.; Duclaux, L.; Grillet, A.-C.; Ha Thuc, H. *J. Nanomater.* **2014**, *2014*, 11.
12. Chen, K. S.; Chen, Y. S.; Yu, T. L.; Tsai, C. L. *J. Polym. Res.* **2002**, *9*, 119.
13. Chen, T. K.; Tien, Y. I.; Wei, K. H. *Polymer* **2000**, *41*, 1345.
14. Chattopadhyay, D. K.; Raju, K. V. S. N. *Prog. Polym. Sci.* **2007**, *32*, 352.
15. Heidarian, M.; Shishesaz, M. R. *J. Appl. Polym. Sci.* **2012**, *126*, 2035.
16. Buckley, C. P.; Prisacariu, C.; Caraculacu, A. *Polymer* **2007**, *48*, 1388.
17. Ma, J.; Zhang, S.; Qi, A. *J. Appl. Polym. Sci.* **2001**, *82*, 1444.
18. Rama, M. S.; Swaminathan, S. *J. Appl. Polym. Sci.* **2010**, *118*, 1774.
19. Huang, W.; Han, C. D. *Polymer* **2006**, *47*, 4400.
20. Jiratumnukul, N.; Manowanna, P.; Premmag, N. *Eng. J.* **2010**, *16*, 13.
21. Brookfield Digital Viscometer Model DV-I+, Brookfield Engineering Laboratories, Manual No: M/92-021-A-892, pp. 18.
22. Hiltz, J. A.; Szabo, J. P. *Defence R&D Canada* **2001**, DREA TM 2001-073.
23. GunaSingh, C.; Soundararajan, S.; Palanivelu, K. *IOSR J. Appl. Chem.* **2013**, *4*, 65.
24. Wang, J.; Iroh, J. O.; Long, A. Controlling the structure and rheology of polyimide/nanoclay composites by in-situ condensation polymerization. *J. Appl. Polym. Sci.* **2012**, *125*, E486.
25. Wang, J.; Iroh, J. O.; Hall, S. Effect of polyaniline modified clay on the processing and properties of clay polyimide nanocomposites. *J. Appl. Clay Sci.* **2014**, *99*, 215.
26. Salomon, D.; Zhai, H. *J. Appl. Asphalt Binder Technol.* **2002**, *2*, 52.
27. Iroh, J. O.; Longun, J. *J. Inorg. Organomet. Polym.* **2012**, *22*, 653.
28. Chiou, B. S.; Schoen, P. E. *J. Appl. Polym. Sci.* **2002**, *83*, 212.